IOPscience iopscience.iop.org

Home Search Collections Journals About Contact us My IOPscience

Study of the phonon–polaritons in piezomagnetic superlattices using a generalized transfer matrix method

This article has been downloaded from IOPscience. Please scroll down to see the full text article.

2006 J. Phys.: Condens. Matter 18 9083

(http://iopscience.iop.org/0953-8984/18/39/034)

View the table of contents for this issue, or go to the journal homepage for more

Download details:
IP Address: 129.252.86.83
The article was downloaded on 28/05/2010 at 14:09

Please note that terms and conditions apply.

INSTITUTE OF PHYSICS PUBLISHING JOURNAL OF PHYSICS: CONDENSED MATTER

J. Phys.: Condens. Matter **18** (2006) 9083–9092 doi:10.1088/0953-8984/18/39/034

Study of the phonon–polaritons in piezomagnetic superlattices using a generalized transfer matrix method

Zhenxing Liu and Weiyi Zhang

Jiangsu Provincial Laboratory for NanoTechnology and National Laboratory of Solid State Microstructures, Nanjing University, Nanjing 210093, People's Republic of China

Received 2 May 2006, in final form 28 July 2006
Published 15 September 2006
Online at stacks.iop.org/JPhysCM/18/9083

Abstract

Piezomagnetic materials are characterized by strong coupling between magnetization and acoustic vibration and the piezomagnetic coefficients change sign with respect to domain polarization. For piezomagnetic superlattices (PMSL) with periodically up and down polarized domain structures, the piezomagnetic coefficients are modulated periodically, and the resulting phonon–polaritons form a band-like structure. This study, using the generalized transfer matrix method, shows that a polariton-like band-gap can be realized in piezomagnetic material with the 6*mm* point group under a certain configuration of magnetic field, lattice displacement and domain polarization, but the mid-gap frequency is restricted to the range of a few GHz or below if the domain wall effect is taken into consideration.

1. Introduction

Wave propagation in bulk media is determined by the dispersion relation of corresponding excitations, and the band-gap in excitation spectra is very useful in providing an 'insulating background' for the modes within that frequency window. The 'insulating background' offers the opportunity for local engineering of microstructures, the modes within the band-gap, by way of specially designed defect-doping, play an important role in guiding wave propagation in the medium, and the architecture of various defect distribution schemes in the medium paves the way for a number of device applications. The most notable example is integrated circuits based on semiconductors, where intrinsic semiconductors are doped locally by n or p type defects to modify the local carrier density and carrier types so that different logic devices can be designed. Motivated by the same logic, Yablonovitch and John [1, 2] proposed the concept of photonic crystals (PC) with an absolute photonic band-gap (PBG) [3–8]; a similar idea was later applied to develop phononic crystals (PhC) [9–12] and other artificially designed structures. However, since the photon wavelength and phonon wavelength are much larger than the lattice constant of the atomic crystal structure, artificially designed structures with

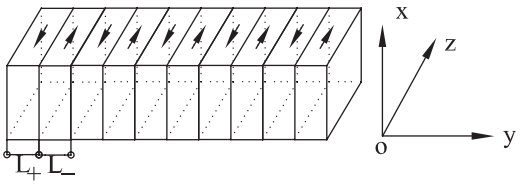

Figure 1. The schematic setup of a piezomagnetic superlattice. L_+ and L_- denote the domain thicknesses and arrows refer to the polarization directions of the domains. Ferromagnetic domains are arranged along the y-axis and the transverse magnetic field is in the z-axis.

periodically modulated dielectric or elastic constants have to be made comparable with the wavelength of the corresponding propagating waves.

Recently, the exploration of band-gap materials was further extended to other mode-coupled systems, in particular the piezoelectric superlattices; these have been studied by several groups and polariton-like band-gap structures have been proposed [13, 14]. It is well known that polariton excitations are the collective modes which result from the coupling between electromagnetic waves and other degrees of freedom in materials. A typical example is the polariton excitations in bulk ionic crystals where the electromagnetic waves interact strongly with the optical phonon vibration; the strong coupling causes the opening of a band-gap in the transmission spectrum near the frequency range where photon dispersion and optical phonon dispersion intersect with each other. The situation in bulk piezoelectric materials is somewhat different since the phenomenon involves an electromagnetic wave and an acoustic wave; both of these have an almost linear dispersion relationship and crossing of the photon and acoustic phonon dispersions never takes place, thus there is no spectral gap opening in the bulk systems. To overcome this difficulty, piezoelectric superlattices with an alternately arranged domain structure are proposed—oppositely polarized ferroelectric domains introduce a modulation in the piezoelectric constant. As a result, the original acoustic phonon dispersion in bulk media is folded because of the reduced Brillouin zone. The coupling between electromagnetic waves and folded 'optical phonons' indeed yields the polariton band-gap just as in the bulk ionic crystals.

In this paper, we have extended our previous rigorous analysis of piezoelectric superlattices to piezomagnetic superlattices. The excitation spectrum of the phonon–polariton in a coupled system has been studied using the transfer matrix method; this method not only yields the full band structures of phonon–polariton excitations, but also explores the coupling information between the external electromagnetic wave and internal eigenmodes and offer a directly measurable quantities such as transmission spectra. The piezomagnetic superlattices we considered here are made of the same type of piezomagnetic material with antiparallel magnetic domains; a representative configuration is schematically illustrated in figure 1. Due to the symmetry requirement of the crystal structure, the piezomagnetic coefficients for the neighbouring antiparallel magnetic domains have opposite signs. The superlattice behaves like a periodic medium modulated by the piezomagnetic coefficient, and thus the original linear dispersion curve of the acoustic phonons is effectively folded back because of the finite Brillouin zone. Now the folded phonon branches can intersect with the photon branch, the conservations of both energy and momentum ensures that strong coupling between photons and phonons can occur in the piezomagnetic superlattice and the polaritonic band-gap can be realized.

Although many studies have been carried out on piezomagnetic materials [15–20], the study of wave propagation in piezomagnetic superlattices is relatively new, and only very few

references exist [20] in which the excitation dispersion curve is solved in the long-wavelength limit. It is of interest to investigate what the dispersion curve looks like in the whole Brillouin zone, and to check the polariton-like band-gap by calculating the transmission spectra directly, since this is the only quantity which justifies the existence of the band-gap. In dealing with piezomagnetic superlattices, an extra precaution has to be taken into consideration concerning the effect of the magnetic domain wall [23, 24]. Piezomagnetic superlattices can be treated as rigid superlattices only if the domain sizes are much larger than the domain wall thickness; this imposes a certain restriction on operating frequencies. To achieve a higher operating frequency one usually chooses piezomagnetic materials with a large anisotropy constant since the domain wall thickness is inversely proportional to the square root of the anisotropy constant. Thus, in this paper cobalt ferrite ($CoFe_2O_4$) is chosen as the piezomagnetic material for superlattices since its anisotropy constant (220×10^3 J m^{-3}) [24] is quite large for this class of materials and the corresponding domain wall thickness is about 560 Å. For an operating frequency of several GHz, the lattice constant of superlattices is of the order of several micrometres, the domain wall thickness is about 1% of the lattice constant and superlattices can be safely approximated as rigid lattices. Another advantage of taking $CoFe_2O_4$ as a candidate is that this material is of the hard magnet type and domain walls are energetically difficult to move. We have also chosen the experimental setting shown in figure 1 because it corresponds to the optimized magneto-mechanical coefficient in $CoFe_2O_4$. In this paper we have used the transfer matrix method to analyse both the polariton-like band structures and the transmission spectra in piezomagnetic superlattices. The band structures and transmission spectra are cross-checked, and the band-gap is shown to exist in the transmission spectra because the in-gap pure phonon modes decouple from the incident electromagnetic wave.

The rest of the paper is organized as follows. In section 2, we first derive the general equation set which governs the propagating behaviour of electromagnetic and acoustic waves in the piezomagnetic superlattices. This differential equation set is then reformulated in terms of the transfer matrix method, and from this the band structures can be easily obtained using the Bloch theorem for infinite periodic superlattices while the transmission spectra can be obtained for finite superlattices after imposing proper boundary conditions. The results for the band structures and transmission spectra are presented in section 3; in particular, we have investigated the coupling of various internal eigenmodes with the external incident wave as well as the size dependence of the polaritonic band-gap in transmission spectra. The conclusion is drawn in section 4.

2. The transfer matrix method and phonon–polariton modes

For the coupling configuration illustrated in figure 1, the direction of propagation of the electromagnetic wave and acoustic wave is taken along the superlattice. We assume that the transverse dimensions are much larger than the thicknesses of the magnetic domains, which are of the same order as the acoustic wavelength, so a one-dimensional model is applicable. The up and down polarized domains have layer thicknesses L_+ and L_-, the piezomagnetic coefficient has opposite signs in these domains because it is a third-rank tensor. As we mentioned in the introduction, the piezomagnetic superlattices are treated as rigid lattices, since the lattice constant is two orders of magnitude larger than the domain wall thickness in the GHz frequency range considered in this paper, and the modulation of piezomagnetic coefficient is assumed to be periodic. For the in-layer polarized magnetic domains (z-axis) shown in figure 1, the transverse magnetic field in the z-axis is coupled to the longitudinal acoustic vibration in the y-axis. Though other configurations are also possible, they are not considered here because they yield a much smaller coupling strength than the configuration considered above.

To describe the wave propagation behaviour in the superlattice depicted in figure 1, we start with the Maxwell equation for an electromagnetic wave and the vibrational equation of an acoustic wave

$$\frac{\partial^2}{\partial y^2}H_z(y,t) = \epsilon_0\epsilon_{33}\frac{\partial^2}{\partial t^2}B_z(y,t), \tag{1a}$$

$$\rho\frac{\partial^2}{\partial t^2}u_y(y,t) = \frac{\partial}{\partial y}Z_2(y,t). \tag{1b}$$

$H_z(y,t)$ and $B_z(y,t)$ are the magnetic field and magnetic induction, $u_y(y,t)$ and $Z_2(y,t)$ are the lattice displacement and stress component. ϵ_{33} and ρ denote the relevant dielectric constant and mass density. For the piezomagnetic crystal $CoFe_2O_4$ with point group $6mm$, the general piezomagnetic tensor q_{ij} ($i = 1, 2, 3$; $j = 1, 2, 3, 4, 5, 6$) only has five non-zero piezomagnetic coefficients. They are $q_{15} = q_{24}$, $q_{31} = q_{32}$ and q_{33}, and only q_{32} is relevant for the configuration shown in figure 1. $B_z(y,t)$ and $Z_2(y,t)$ are related to $H_z(y,t)$ and $u_y(y,t)$ via the piezomagnetic effect

$$B_z(y,t) = q_{31}(y)\frac{\partial}{\partial y}u_y(y,t) + \mu_0\mu_{33}H_z(y,t), \tag{2a}$$

$$Z_2(y,t) = c_{22}\frac{\partial}{\partial y}u_y(y,t) - q_{31}(y)H_z(y,t). \tag{2b}$$

Here, c_{22} and μ_{33} are the elastic moduli and permittivity, respectively. These equations suggest that the transverse magnetic field H_z induces the longitudinal lattice vibration u_y and the corresponding polariton results from such coupling.

Substituting equation (2) into (1), one arrives at a set of coupled equations for the magnetic field and lattice displacement

$$\epsilon_0\mu_0\epsilon_{33}\mu_{33}\frac{\partial^2}{\partial t^2}H_z(y,t) = \frac{\partial^2}{\partial y^2}H_z(y,t) - \epsilon_0\epsilon_{33}q_{31}(y)\frac{\partial^3}{\partial t^2\partial y}u_y(y,t), \tag{3a}$$

$$\rho\frac{\partial^2}{\partial t^2}u_y(y,t) = c_{22}\frac{\partial^2}{\partial y^2}u_y(y,t) - \frac{\partial}{\partial y}\left(q_{31}(y)H_z(y,t)\right). \tag{3b}$$

For piezomagnetic superlattices, the piezomagnetic coefficient is polarization dependent and $q_{31}(y) = q_{31}\theta(y)$, the sign function $\theta(y) = \pm 1$ for up and down polarized domains. By defining the velocity of light in a vacuum $c^2 = 1/\epsilon_0\mu_0$ and the velocity of sound $c_s^2 = c_{22}/\rho$, this equation set can be further cast into a dimensionless form after making the variable replacement $y = \bar{y}L/2\pi$, $u_y(y,t) = \bar{u}_y(\bar{y},t)L/2\pi$, and $\bar{H}_z(\bar{y},t) = q_{31}H_z(y,t)/c_{22}$. The final equation set takes the form

$$\bar{\omega}^2\bar{H}_z(\bar{y},\bar{\omega}) + \alpha\frac{\partial^2}{\partial\bar{y}^2}\bar{H}_z(\bar{y},\bar{\omega}) + \bar{\omega}^2\beta\theta(\bar{y})\frac{\partial}{\partial\bar{y}}\bar{u}_y(\bar{y},\bar{\omega}) = 0, \tag{4a}$$

$$\bar{\omega}^2\bar{u}_y(\bar{y},\bar{\omega}) + \frac{\partial^2}{\partial\bar{y}^2}\bar{u}_y(\bar{y},\bar{\omega}) - \frac{\partial}{\partial\bar{y}}[\theta(\bar{y})\bar{H}_z(\bar{y},\bar{\omega})] = 0. \tag{4b}$$

Here $\bar{A}$ is the corresponding quantity of A in a dimensionless form, $\bar{A}(\bar{y},\bar{\omega})$ is a Fourier transformed quantity of $\bar{A}(\bar{y},t)$, L is lattice constant of the piezomagnetic superlattice and is the sum of two oppositely polarized domains, the reduced lattice constant is 2π. $\bar{\omega} = \omega L/2\pi c_s$ is the reduced frequency of the eigensystem under study. $\alpha = c^2/c_s^2\epsilon_{33}\mu_{33}$, and $\beta = q_{31}^2/\mu_0\mu_{33}c_{22}$ is magneto-mechanical transducer coefficient which describes the coupling

strength between photons and phonons. For superlattices composed of $CoFe_2O_4$ ferromagnetic materials [21, 22], the domain wall thickness is about 560 Å. If the lattice constant is of the order of a few micrometres, which is two orders of magnitude higher than the domain wall thickness, then the corresponding frequency is in the range of several GHz; the value of permeability in this frequency range is around $\mu_{33} \approx 2$ [22]. The two dynamical parameters are estimated to be $\alpha = 0.7882 \times 10^8$, $\beta = 0.4687$ for the configuration shown in figure 1. Since the parameter $\beta = q_{31}^2/\mu_0\mu_{33}c_{22}$ determines the coupling strength between the electromagnetic wave and acoustic wave, and thus ultimately determines the size of polaritonic band-gap, it is desirable to choose the proper material and configuration setting which yields the largest magneto-mechanical transducer coefficient in the required frequency range. We would like to mention in passing that the photon velocity is four orders of magnitude higher than the sound velocity (see α coefficient), and their wavelengths set two different characteristic length scales in the bulk piezomagnetic system.

The above differential equations can be recast in terms of the transfer matrix method. By solving the eigensolutions in the homogeneously up and down polarized domains, the general solution in superlattices can be expressed within these bases. Using the boundary conditions that the magnetic field $\bar{H}_z(\bar{y}, \bar{\omega})$, displacement $\bar{u}_y(\bar{y}, \bar{\omega})$, the derivative of magnetic field $\mathrm{d}\bar{H}_z(\bar{y}, \bar{\omega})/\mathrm{d}\bar{y}$ and stress component $Z_2(\bar{y}, \bar{\omega})/c_{22} = \mathrm{d}\bar{u}_y(\bar{y}, \bar{\omega})/\mathrm{d}\bar{y} - \theta(\bar{y})\bar{H}_z(\bar{y}, \bar{\omega})$ are continuous across the domain interface, one can define the transfer matrix in each domain which relates the fields and their derivatives at the two sides of a domain

$$\begin{pmatrix} \bar{H}_z(\bar{L}_\pm, \bar{\omega}) \\ \bar{u}_y(\bar{L}_\pm, \bar{\omega}) \\ \bar{H}_z'(\bar{L}_\pm, \bar{\omega}) \\ \bar{u}_y'(\bar{L}_\pm, \bar{\omega}) \mp \bar{H}_z(\bar{L}_\pm, \bar{\omega}) \end{pmatrix} = M(\bar{L}_\pm, \bar{\omega}) \begin{pmatrix} \bar{H}_z(\bar{0}, \bar{\omega}) \\ \bar{u}_y(\bar{0}, \bar{\omega}) \\ \bar{H}_z'(\bar{0}, \bar{\omega}) \\ \bar{u}_y'(\bar{0}, \bar{\omega}) \mp \bar{H}_z(\bar{0}, \bar{\omega}) \end{pmatrix}. \tag{5}$$

The detailed expressions of the transfer matrices $M(\bar{L}_\pm, \bar{\omega})$ are listed in the appendix. Here upper and lower signs denote the up and down polarized domains. The transfer matrix of a superlattice can be obtained by successive application of $M(\bar{L}_\pm, \bar{\omega})$ using the sequence depicting superlattice configuration. This forms the basis for studying the band structures and transmission spectra of the superlattices.

For example, the band structures can be calculated easily using the Bloch theorem. In this case, we need to solve the following matrix equation

$$M(\bar{L}_+, \bar{\omega})M(\bar{L}_-, \bar{\omega}) = \exp(\mathrm{i}\bar{k}\bar{L})I \tag{6}$$

with I and $\bar{k}$ denoting the 4×4 unit matrix and reduced wavenumber. To compute the transmission and reflection spectra of a finite superlattice with number of periods NP, the global transfer matrix is given by

$$M = [M(\bar{L}_+, \bar{\omega})M(\bar{L}_-, \bar{\omega})]^{\mathrm{NP}}. \tag{7}$$

For the longitudinal vibrational mode illustrated in figure 1, the huge imbalance of acoustic impedance between air and the bulk ferromagnetic medium effectively blocks the propagation of acoustic wave between them, and the boundaries at the two outer surfaces are stress free. The amplitudes of the transmission t and reflection r can be expressed in terms of the global transfer matrix elements M_{ij} as follows

$$t = \frac{2M_{42}}{M_{42}[(M_{11} + f_pM_{13}) + f_p^{-1}(M_{31} + f_pM_{33})] - (M_{12} + f_p^{-1}M_{32})(M_{41} + f_pM_{43})}, \tag{8a}$$

$$r = \frac{M_{42}[(M_{11} + f_pM_{13}) - f_p^{-1}(M_{31} + f_pM_{33})] - (M_{12} - f_p^{-1}M_{32})(M_{41} + f_pM_{43})}{M_{42}[(M_{11} + f_pM_{13}) + f_p^{-1}(M_{31} + f_pM_{33})] - (M_{12} + f_p^{-1}M_{32})(M_{41} + f_pM_{43})}, \tag{8b}$$

and the parameter $f_p = \mathrm{i}c_s\bar{\omega}/c$. The experimentally measured transmission and reflection spectra are given by $T = |t|^2$ and $R = |r|^2$; they satisfy the energy conservation law $R+T = 1$ in the absence of dissipation by the medium.

3. Numerical results and discussions

Before we investigate the mode-coupling and gap-opening mechanism in piezomagnetic superlattices, it is useful to recall how the electronic band-gaps are created from the free electron picture in periodic crystal structures. The gap opening is determined by the following two criteria: (1) doubly degenerate electronic states exist for two wavevectors $\bar{k}$ and $\bar{k}' = \bar{k}+\bar{K}_n$ which are connected by a reciprocal lattice vector $\bar{K}_n$; (2) these two degenerate states are coupled by the corresponding Fourier component of electronic potential $\theta(\bar{K}_n)$. For electronic systems, degenerate energy states usually occur either at the boundary or at the centre of Brillouin zones; these are usually where the band-gaps are created. In contrast to electronic systems, the creation of a band-gap in a piezomagnetic superlattice is somewhat different: (1) there are two degrees of freedom representing the electromagnetic wave and the vibrational wave; (2) direct coupling only takes place between different degrees of freedom. Thus, a band-gap can be created only in those reduced wavevectors where dispersion curves for photons and phonons intersect with each other. Since the velocity of light is four orders of magnitude larger than the phonon velocity, the photon wavenumber is very small in the frequency range of interest and the band-gap only occurs near the Brillouin centre. Therefore, in order to have a polariton-like band-gap near the Brillouin centre, one needs to have nonzero Fourier components for the coupling coefficient at the frequency where photon and phonon modes intersect.

For the symmetrical configuration where the up and down polarized domains have equal layer thickness, the Fourier components of the structure factor are nonzero only for odd reciprocal lattice vectors; thus the band-gaps are expected to occur only near the frequency $\bar{\omega} = 1, 3, 5$ etc. To check the above physical analysis, the band structures are calculated from equation (6) for the symmetrical configuration and the dispersion relations of phonon–polaritons are shown in figure 2. The horizontal axis denotes the reduced frequency while the vertical axis is the reduced wavenumber. The solid circles represent the real wavenumber while the open triangles represent the imaginary wavenumber and thus signify the polaritonic band-gap region. The wavenumber is either purely real or purely imaginary since there is no absorption in this problem. Figure 2(a) shows the overall band structure in the whole Brillouin zone, and the dispersion relation can be viewed as simply the folded dispersion relation of an acoustic wave in a homogeneous medium; the proposed polariton-like band-gap is not visible in the figure. The fact that $\sqrt{\alpha} \simeq 10^4$ (ratio of the photon velocity and sound velocity) reminds us that a significant coupling takes place only near the centre of Brillouin zone. This part of the dispersion curve is enlarged and replotted in figure 2(b). We find that polariton-like band-gaps do appear when $\omega L/2\pi c_s$ equals odd integers as predicted in our simple physical analysis, though the sizes of the band-gaps decrease rapidly as the middle gap frequency increases. Figure 2 suggests that there are two independent dispersion curves: the dispersion curve for large wavenumbers corresponds to that of a folded acoustic phonon while those at very small wavenumbers are polariton modes due to mixing between photons and phonons. The size of the polariton band-gap is proportional to the coupling strength. It should be emphasized that the polariton band-gap exists only in one of the dispersion curves; the modes of other dispersion curve are actually present in this gap, but these gap modes can be shown to be decoupled from the external incident electromagnetic wave and are evident in our calculated transmission spectra.

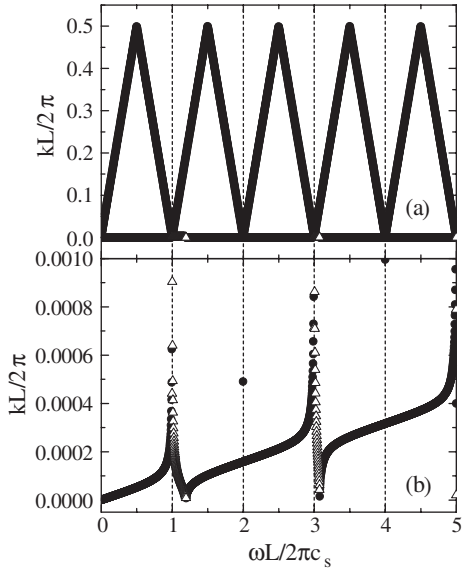

Figure 2. The polariton-like band structures for a symmetrical piezomagnetic superlattice. The reduced domain thicknesses are $\bar{L}_+ = \bar{L}_- = \pi$ and the material parameters are listed in the text. (a) For the whole Brillouin zone. (b) Near the centre of the Brillouin zone. Open triangles represent the imaginary wavenumbers and the gap region while the solid circles represent real wavenumbers and the pass band.

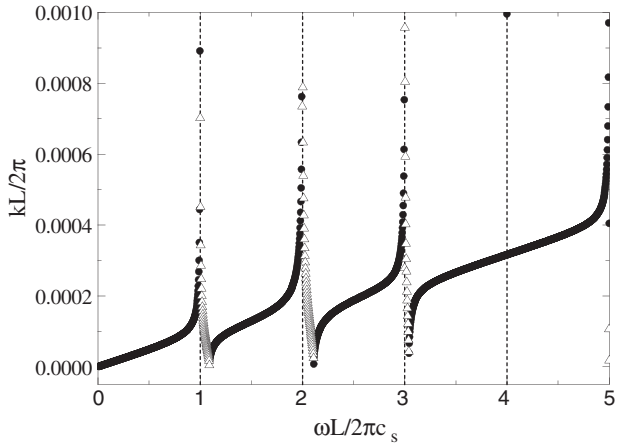

Figure 3. The polariton-like band structures for an asymmetrical piezomagnetic superlattice near the centre of the Brillouin zone. $\bar{L}_+ = 0.5\pi$ and $\bar{L}_- = 1.5\pi$. The other parameters and notation are the same as in figure 2.

When the layer thicknesses of up and down polarized domains are different, the Fourier components of the structure factor survive for all reciprocal lattice vectors and polaritonic band-gaps can occur at both odd and even integer values of reduced frequencies. As an example, the band structures for the reduced domain thicknesses $\bar{L}_+ = 0.5\pi$ and $\bar{L}_- = 1.5\pi$ are computed and the results are plotted in figure 3. As shown by the polaritonic band-gaps indicated by the open triangles, though the band-gaps are now present for more integer frequencies, the sizes of

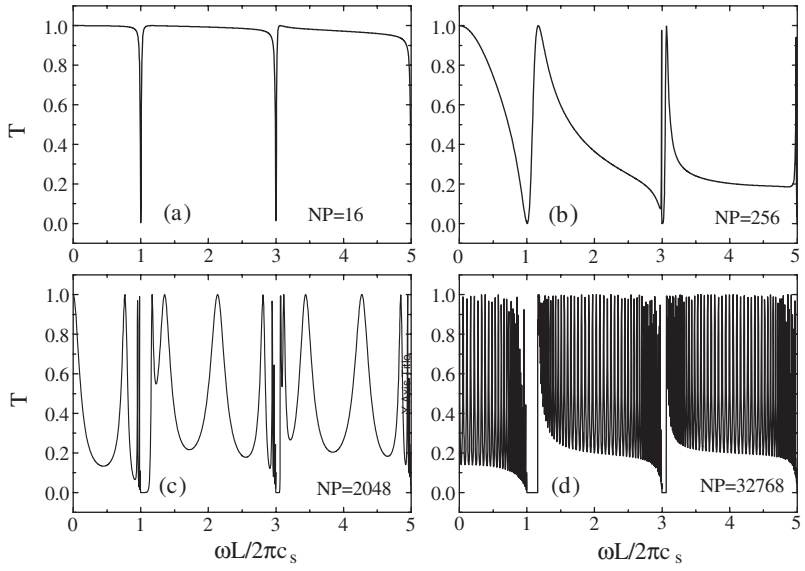

Figure 4. Transmission spectra for symmetrical piezomagnetic superlattices: (a) 16 periods, (b) 256 periods, (c) 2048 periods, (d) 32 768 periods. Since reflection and transmission coefficients satisfy the sum rule, only transmission coefficients are shown. The other parameters are the same as those in figure 2.

the gaps are drastically reduced due to the reduced Fourier components of the piezomagnetic coefficient.

To make sure that the polaritonic band-gaps are genuine, one has to show that the in-gap modes do decouple from the external incident wave. This can be done by computing the transmission and reflection spectra of finite superlattices using the generalized transfer matrix method. As we mentioned in the previous section, the huge imbalance in acoustic impedance between air and the bulk ferromagnetic medium effectively blocks the propagation of acoustic waves across the outer surfaces of a finite sample, and the boundaries at the two outer surfaces can be assumed to be stress free. The resulting transmission spectra are shown in figure 4 for four different numbers of lattice periods (NP). The transmission spectra change dramatically with the sample thickness, but the polaritonic band-gap already demonstrates its existence at a lattice period NP $= 16$. The appearance of the band-gap is first illustrated as a dip in the transmission spectra (NP $= 16$), its width increases with the lattice period and saturates when the lattice period approaches several thousands of layers and beyond. From the transmission spectrum plotted in figure 4(d), the relative gaps (the gap divided by the mid-gap frequency) are 15% and 2.1% for the first and second gaps, respectively and they are in very good agreement with those obtained from the band structures. Note that the rapid oscillations within the pass bands of the spectra are due to the finite sample length and thus the Fabry–Perot interference effect within the samples. These calculated transmission spectra also offer useful guidance on sample preparation in order to observe the sizable polariton-like band-gap experimentally.

4. Conclusion

In summary, the band structure and propagating behaviour of electromagnetic (EM) waves in piezomagnetic superlattices are studied using the generalized transfer matrix method,

and the polaritonic band-gaps are predicted and cross-checked from the dispersion relations and transmission spectra. For a piezomagnetic superlattice made of $CoFe_2O_4$ crystal with point group 6*mm*, the polaritonic band-gaps result from the mode coupling between an electromagnetic wave and a longitudinal acoustic wave and the relative gaps (gap divided by mid-gap frequency) are 15% and 2.1% for the first and second gaps, respectively. In addition, we show that the band-gap increases with the lattice period and the band-gap saturates when the lattice period approaches several thousand layers. The above results are obtained within the framework of a rigid superlattice model which holds approximately in the frequency range of a few GHz or below.

Acknowledgments

This work was supported in part by the State Key Program for Basic Research of China (grant no 2004CB619003). We wish to acknowledge partial financial support from the NNSFC under grant no 10474040, 10334090, 10523001 and the 'Excellent Youth Foundation' [10025419].

Appendix. Transfer matrices for two polarized domains

$c_\pm = \sqrt{0.5[(\alpha+\beta+1) \pm \sqrt{(\alpha+\beta+1)^2 - 4\alpha}]}$ are the reduced velocities for photons and phonons, respectively. $\bar{\omega} = \omega L/2\pi c_s$, $\bar{L}_\pm = 2\pi L_\pm/L$. The sub-index $\pm$ represents two polarized domains.

$$M(\bar{L}_\pm, \bar{\omega}, 1, 1) = \frac{1}{(c_+^2 - c_-^2)}\left[c_-^2(c_+^2-1)\cos\frac{\bar{\omega}\bar{L}_\pm}{c_+} - c_+^2(c_-^2-1)\cos\frac{\bar{\omega}\bar{L}_\pm}{c_-}\right] \tag{A.1}$$

$$M(\bar{L}_\pm, \bar{\omega}, 1, 2) = \frac{\mp(c_+^2-1)(c_-^2-1)\bar{\omega}}{(c_+^2 - c_-^2)}\left[c_+\sin\frac{\bar{\omega}\bar{L}_\pm}{c_+} - c_-\sin\frac{\bar{\omega}\bar{L}_\pm}{c_-}\right] \tag{A.2}$$

$$M(\bar{L}_\pm, \bar{\omega}, 1, 3) = \frac{c_+c_-}{(c_+^2 - c_-^2)\bar{\omega}}\left[c_-(c_+^2-1)\sin\frac{\bar{\omega}\bar{L}_\pm}{c_+} - c_+(c_-^2-1)\sin\frac{\bar{\omega}\bar{L}_\pm}{c_-}\right] \tag{A.3}$$

$$M(\bar{L}_\pm, \bar{\omega}, 1, 4) = \frac{\pm(c_+^2-1)(c_-^2-1)}{(c_+^2 - c_-^2)}\left[\cos\frac{\bar{\omega}\bar{L}_\pm}{c_+} - \cos\frac{\bar{\omega}\bar{L}_\pm}{c_-}\right] \tag{A.4}$$

$$M(\bar{L}_\pm, \bar{\omega}, 2, 1) = \mp\frac{c_+c_-}{(c_+^2 - c_-^2)\bar{\omega}}\left[c_-\sin\frac{\bar{\omega}\bar{L}_\pm}{c_+} - c_+\sin\frac{\bar{\omega}\bar{L}_\pm}{c_-}\right] \tag{A.5}$$

$$M(\bar{L}_\pm, \bar{\omega}, 2, 2) = \frac{-1}{(c_+^2 - c_-^2)}\left[c_+^2(c_-^2-1)\cos\frac{\bar{\omega}\bar{L}_\pm}{c_+} - c_-^2(c_+^2-1)\cos\frac{\bar{\omega}\bar{L}_\pm}{c_-}\right] \tag{A.6}$$

$$M(\bar{L}_\pm, \bar{\omega}, 2, 3) = \frac{\pm c_+^2c_-^2}{(c_+^2 - c_-^2)\bar{\omega}^2}\left[\cos\frac{\bar{\omega}\bar{L}_\pm}{c_+} - \cos\frac{\bar{\omega}\bar{L}_\pm}{c_-}\right] \tag{A.7}$$

$$M(\bar{L}_\pm, \bar{\omega}, 2, 4) = \frac{-1}{(c_+^2 - c_-^2)\bar{\omega}}\left[c_+(c_-^2-1)\sin\frac{\bar{\omega}\bar{L}_\pm}{c_+} - c_-(c_+^2-1)\sin\frac{\bar{\omega}\bar{L}_\pm}{c_-}\right] \tag{A.8}$$

$$M(\bar{L}_\pm, \bar{\omega}, 3, 1) = \frac{-\bar{\omega}}{c_+c_-(c_+^2 - c_-^2)}\left[c_-^3(c_+^2-1)\sin\frac{\bar{\omega}\bar{L}_\pm}{c_+} - c_+^3(c_-^2-1)\sin\frac{\bar{\omega}\bar{L}_\pm}{c_-}\right] \tag{A.9}$$

$$M(\bar{L}_\pm, \bar{\omega}, 3, 2) = \frac{\mp(c_+^2-1)(c_-^2-1)\bar{\omega}^2}{(c_+^2 - c_-^2)}\left[\cos\frac{\bar{\omega}\bar{L}_\pm}{c_+} - \cos\frac{\bar{\omega}\bar{L}_\pm}{c_-}\right] \tag{A.10}$$

$$M(\bar{L}_\pm, \bar{\omega}, 3, 3) = \frac{1}{(c_+^2 - c_-^2)}\left[c_-^2(c_+^2-1)\cos\frac{\bar{\omega}\bar{L}_\pm}{c_+} - c_+^2(c_-^2-1)\cos\frac{\bar{\omega}\bar{L}_\pm}{c_-}\right] \tag{A.11}$$

$$M(\bar{L}_{\pm},\bar{\omega},3,4)=\frac{\mp(c_{+}^{2}-1)(c_{-}^{2}-1)\bar{\omega}}{c_{+}c_{-}(c_{+}^{2}-c_{-}^{2})}\left[c_{-}\sin\frac{\bar{\omega}\bar{L}_{\pm}}{c_{+}}-c_{+}\sin\frac{\bar{\omega}\bar{L}_{\pm}}{c_{-}}\right] \tag{A.12}$$

$$M(\bar{L}_{\pm},\bar{\omega},4,1)=\frac{\mp c_{+}^{2}c_{-}^{2}}{(c_{+}^{2}-c_{-}^{2})}\left[\cos\frac{\bar{\omega}\bar{L}_{\pm}}{c_{+}}-\cos\frac{\bar{\omega}\bar{L}_{\pm}}{c_{-}}\right] \tag{A.13}$$

$$M(\bar{L}_{\pm},\bar{\omega},4,2)=\frac{\bar{\omega}}{(c_{+}^{2}-c_{-}^{2})}\left[c_{+}^{3}(c_{-}^{2}-1)\sin\frac{\bar{\omega}\bar{L}_{\pm}}{c_{+}}-c_{-}^{3}(c_{+}^{2}-1)\sin\frac{\bar{\omega}\bar{L}_{\pm}}{c_{-}}\right] \tag{A.14}$$

$$M(\bar{L}_{\pm},\bar{\omega},4,3)=\frac{\mp c_{+}^{2}c_{-}^{2}}{(c_{+}^{2}-c_{-}^{2})\bar{\omega}}\left[c_{+}\sin\frac{\bar{\omega}\bar{L}_{\pm}}{c_{+}}-c_{-}\sin\frac{\bar{\omega}\bar{L}_{\pm}}{c_{-}}\right] \tag{A.15}$$

$$M(\bar{L}_{\pm},\bar{\omega},4,4)=\frac{-1}{(c_{+}^{2}-c_{-}^{2})}\left[c_{+}^{2}(c_{-}^{2}-1)\cos\frac{\bar{\omega}\bar{L}_{\pm}}{c_{+}}-c_{-}^{2}(c_{+}^{2}-1)\cos\frac{\bar{\omega}\bar{L}_{\pm}}{c_{-}}\right]. \tag{A.16}$$

References

[1] Yablonovitch E 1987 *Phys. Rev. Lett.* **58** 2059
[2] John S 1987 *Phys. Rev. Lett.* **58** 2486
[3] Yablonovitch E, Gmitter T J and Bhat R 1988 *Phys. Rev. Lett.* **61** 2546
[4] Ho K M, Chan C T and Soukoulis C M 1990 *Phys. Rev. Lett.* **65** 3152
[5] Karathanost V, Modinos A and Stefanou N 1994 *J. Phys.: Condens. Matter* **6** 6257
[6] Busch K and John S 1998 *Phys. Rev.* E **58** 3896
[7] Fan S, Villeneuve P R and Joannopoulos J D 1996 *Phys. Rev.* B **54** 11245
[8] Zhang W, Lei X Y, Wang Z L, Zheng D G, Tam W Y, Chan C T and Sheng P 2000 *Phys. Rev. Lett.* **84** 2853
[9] Kushwaha M S, Halevi P, Dobrzynski L and Djafari-Rouhani B 1993 *Phys. Rev. Lett.* **71** 2022
[10] Sánchev-Pérez J V, Caballero D, Martinez-Sala R, Rubio C, Sánchev-Dehesa J, Meseguer F, Llinares J and Galvez F 1998 *Phys. Rev. Lett.* **80** 5325
[11] Montero de Espinosa F R, Jiménez E and Torres M 1998 *Phys. Rev. Lett.* **80** 1208
[12] Goffaux C, Sanchez-Dehesa J, Levy Yeyati A, Lambin Ph, Khelif A, Vasseux J O and Djafari-Rouhani B 2002 *Phys. Rev. Lett.* **88** 225502
[13] Lu Y, Zhu Y, Chen Y, Zhu S, Ming N and Feng Y 1999 *Science* **284** 1822
[14] Zhang X, Zhu R-Q, Zhao J, Chen Y and Zhu Y 2004 *Phys. Rev.* B **69** 085118
[15] Alshits V I and Shuvalov A L 1993 *Phys. Lett.* A **177** 253
[16] Alshits V I and Shuvalov A L 1993 *JETP* **76** 663
[17] Bichurin M I, Petrov V M, Kiliba Yu V and Srinivasan G 2002 *Phys. Rev.* B **66** 134404
[18] Bichurin M I, Filippov D A, Petrov V M, Laletsin V M, Paddubnaya N and Srinivasan G 2003 *Phys. Rev.* B **68** 132408
[19] Zheng H, Wang J, Lofland S E, Ma Z, Mohaddes-Ardabili L, Zhao T, Salamanca-Riba L, Shinde S R, Ogale S B, Bai F, Viehland D, Jia Y, Schlom D G, Wuttig M, Roytburd A and Ramesh R 2004 *Science* **303** 661
[20] Liu H, Zhu S N, Dong Z G, Zhu Y Y, Chen Y F and Ming N B 2005 *Phys. Rev.* B **71** 125106
[21] Huang J H and Kuo W-S 1997 *J. Appl. Phys.* **81** 1378
[22] Bichurin M I, Petrov V M and Srinivasan G 2003 *Phys. Rev.* B **68** 054402
[23] Slick P I 1980 *Ferromagnetic Materials* vol 2, ed E P Wohlfarth (Amsterdam: North-Holland)
[24] Chen C W 1977 *Magnetism and Metallurgy of Soft Magnetic Materials* vol 15, ed E P Wohlfarth (Amsterdam: North-Holland)